Received 30 June 2022; accepted 2 August 2022. Date of publication 16 August 2022; date of current version 25 August 2022.

Digital Object Identifier 10.1109/OJAP.2022.3198289

Indigenously Developed HD Video Transmission System for UAVs Employing a 3 × 3 MIMO Antenna System

ZUBAIR AKHTER (Member, IEEE), RANA M. BILAL, KUAT TELEGENOV, ERIC FERON, AND ATIF SHAMIM (Senior Member, IEEE)

Electrical and Computer Engineering Program, CEMSE Division, King Abdullah University of Science and Technology, Thuwal 23955, Saudi Arabia

CORRESPONDING AUTHOR: Z. AKHTER (e-mail: zubair.akhter@kaust.edu.sa)

ABSTRACT Real-time high-definition (HD) video transmission for long distances (≥1 km) between an unmanned aerial vehicle (UAV) and a ground station is a challenging problem. The existing real-time solutions are limited to relatively low-quality video streaming, whereas an HD video, which is stored in the local memory, is accessible only when the UAV returns to the ground. In this study, a real-time HD video transmission system (VTS) with a multiple-input multiple-output (MIMO) antenna configuration and state-of-the-art coverage is proposed for security and inspection applications. The proposed VTS employs ultrathin, lightweight antennas that are suitable for seamless integration with a UAV's body without any protrusion. A 3 × 3 MIMO configuration with large antenna bandwidths (3.9% at 2.4 GHz and 6.9% at 5.2 GHz) enables the simultaneous transmission of multiple data streams with high data rates (>30 Mbps), and a high antenna gain (∼10 dBi) allows a relatively long communication range (>3 km). In field experiments, the UAV module (comprising thin conformal antennas, embedded electronics, an RF transceiver, and an HD camera) is attached to a commercial drone DJI Matrice 600 Pro. The HD video's reception performance is investigated for operation in two frequency bands (2.4 and 5.2 GHz) for both horizontal and vertical antenna orientations. The maximum and average data rates for various distances are reported. Based on the conducted field experiments, it is found that the proposed VTS is capable of transmitting real-time HD video up to a 3.56-km distance with a receiver sensitivity of −76 dBm. The maximum achieved data rates at a 500-m distance are ∼10 and ∼43 Mbps for operation in the 2.4- and 5.2-GHz frequency bands, respectively.

INDEX TERMS Inspection, HD video, MIMO, UAV, streaming, security.

I. INTRODUCTION

UNMANNED aerial vehicles (UAVs), also known as drones, have been used in various applications, such as aerial photography, search and rescue, precision agriculture, pipeline/overhead transmission-line monitoring, aerial mapping, wildlife monitoring, surveillance, disaster management, and delivery of medical supplies [1], [2], [3], [4], [5], [6], [7], [8], [9], [10], [11], [12], [13], [14], [15], [16], [17], [18]. Depending on the requirements of such applications, UAVs are equipped with various types of sensors and modules for transmitting sensed/acquired data to a remotely located control/ground station. In addition, real-time high-definition (HD) video transmission of a scene is also becoming an asset for drones. Significant reports on video transmission systems (VTSs) have been recently published [19], [20], [21], [22], [23]. However, the air-to-ground transmission poses several challenges due to diverse environmental conditions, such as signal fading, attenuation, interference, and obstacles. In addition, the available link budget [24], [25] and antenna performance can affect the transmission range [26].

Currently, the popular choices for UAV antennas are blade antennas, wire monopoles, printed and conformal monopoles or dipoles, annular slot antennas [27], [28], [29], [30], [31],

etc. Blade or wire monopole antennas require an aerodynamic enclosure, which increases the payload and affects the antenna gain. In contrast, thin monopoles/dipoles can directly be attached to a drone's body seamlessly. However, their key performance parameters (i.e., resonance frequency and bandwidth) are sensitive to the electrical properties of the platform material. Conformal monopoles have been used to address the platform sensitivity issue by employing a full ground plane. However, they suffer from narrow bandwidths and large thicknesses [28], [30]. The cavity-backed annular slot antennas provide better platform insensitivity due to the presence of a full ground plane. However, this type and other types, such as the printed/conformal monopoles, exhibit relatively low gains (approximately 1.0–2.5 dBi) [28], [29], [32].

The above discussion indicates that the commonly used UAV antennas exhibit low gains because they are designed for omnidirectional coverage under a single-input single-output approach. Therefore, their communication range is limited by the available link budget. Specifically, their communication range is restricted to a few hundred meters in point-to-point communication on private/ad-hoc networks [33]. This range can be increased by employing repeater/relay nodes on the ground [34] or a swarm of multiple UAVs to create an ad-hoc network [35]. Infrastructure networks, such as the GSM, 3G, and 4G, can also be used to increase the communication range [36], [37], [38]. In this study, we focus on point-to-point communication without using any external network infrastructure (such as GSM, 3G, and 4G) or a network cloud (repeaters or a swarm of drones). Instead, to increase the communication range and capacity, we aim to use directional antennas in an MIMO configuration. In this study, the communication range is increased using conformal high-gain antennas (with ∼6-dB more gain compared to conventional UAV antennas) and the data rate is enhanced by forming multiple data streams using a 3 × 3 MIMO configuration. In addition, the proposed antennas are ultrathin ($0.0128\lambda_0$) and conformal and can be seamlessly mounted on any surface without requiring any aerodynamic enclosure. The proposed VTS is capable of transmitting an HD video in two operating frequency bands (2.4 and 5.2 GHz) under different antenna orientations. Various field experiments for ground-to-ground and air-to-ground connectivity scenarios are conducted. The feasibility of the proposed system is presented in the following section.

II. PROPOSED VIDEO TRANSMISSION SYSTEM

The proposed VTS consists of UAV and ground modules. A conceptualized representation of the VTS is shown in Fig. 1, where the UAV module captures the HD video feed and then compresses and encodes it for transmission to a ground station through a 3-channel MIMO link. The ground station receives, processes, and displays the HD video stream received from the UAV module. The ground station module is equipped with a graphical user interface, which is used to select the network parameters such as frequency band, encoding scheme, and video stream reception initiation.

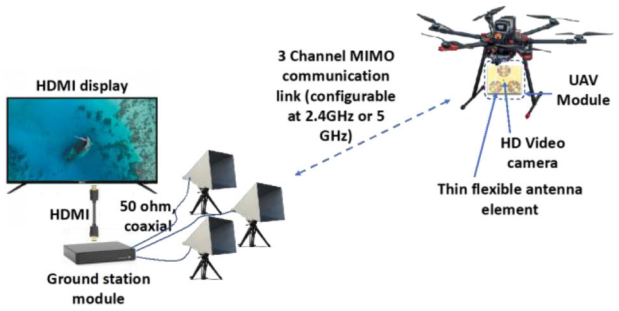

FIGURE 1. Pictorial representation of the proposed high-definition video data transmission system.

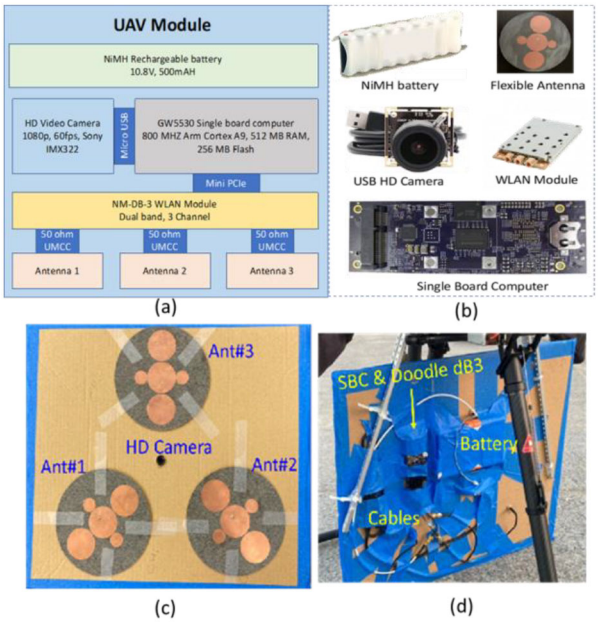

FIGURE 2. (a) Block diagram of the unmanned aerial vehicle (UAV) module, (b) UAV module components, (c) front view of the assembled UAV module/system, and (d) back view of the assembled UAV module/system.

A. UAV AND GROUND (BASE) MODULE SYSTEM ARCHITECTURE

The block diagram and the UAV module's components are shown in Fig. 2. The UAV module as shown in Fig. 2(a) employs a Gateworks GW5530 single-board computer (SBC). The SBC comprises an 800-MHz dual-core Arm cortex A9 processor, coupled with a 512-Mbyte DDR3 RAM, a 256-Mbyte flash memory, a mini PCIe, a mini HDMI, and micro USB ports in a miniature form (3.5 cm × 10 cm). This miniature structure allows easy integration with UAVs. The mini PCIe slot on the Gateworks SBC is used to connect the Doodle's NM-DB-3 WLAN module as shown in Fig. 2(b), which is a three-channel WLAN module. In addition, the UAV module includes an HD video camera connected as shown in Fig. 2(b) to a micro USB port, a battery, and three custom designed antennas as

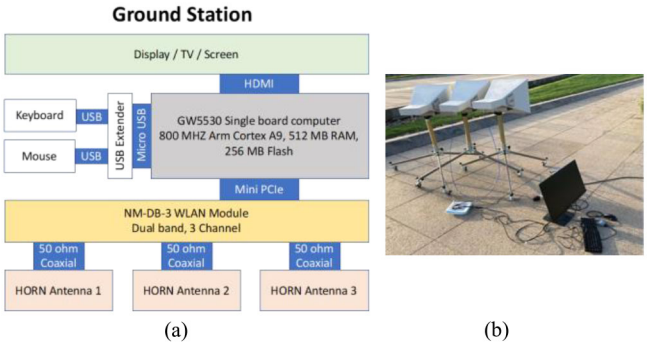

FIGURE 3. (a) Block diagram and (b) picture of ground station.

shown in Fig. 2 (b). These antennas are connected to the radio frequency (RF) ports of the NM-DB-3 module using 50-ohm coaxial cables. The complete UAV module (front and back view) is shown in Fig. 2(c)-(d). A NiMH 10.8-V and 500-mAh rechargeable battery is used to power the UAV module, providing backup power of approximately 60 min at the maximum RF power out setting. The UAV module uses a customized OpenWRT-based firmware running on the SBC. When the UAV module is powered, this firmware boots the hardware initializes all drivers and interfaces and reads the video data stream from the HD camera connected to a micro USB port. The ground station transmits commands to configure the frequency band (2.4 or 5.2 GHz), Wi-Fi channel and its parameters (i.e., bandwidth and guard interval), encoding scheme (modulation and coding scheme (MCS) number), transmitted power, SSID, authentication protocol, authentication credentials, and command to start the video stream. Upon receiving the "start video stream" command, the UAV module starts reading the stream data from the HD camera. Then, it compresses the data using the H.264 compression standard, encodes the data for transmission, and sends the encoded, compressed data stream to the ground station through the WLAN communication link.

Furthermore, the ground station is using the same SBC module (i.e., GW5530) and WLAN card (i.e., NM-DB-3) connected to the PCIe slot on the SBC, as shown in Fig. 4. In addition, the ground station module has an HDMI display connected to the mini HDMI port on the SBC and a keyboard and mouse connected to a micro USB port using a USB extender. Three commercial horn antennas are connected to the RF ports of the WLAN module using 50-ohm coaxial cables. The ground station (i.e., SBC and HDMI display) is powered using a portable generator and wall socket.

B. DUAL MODE ANTENNA DESIGN AND 3×3 MIMO CONFIGURATION

The proposed antenna is a circular patch resonating at two modes (i.e. TM_{11} and TM_{01}) at 2.4 GHz and 5.2 GHz bands simultaneously. The antenna is composed of one driven patch positioned in the center and four parasitic patches around the driven patch as shown in Fig. 4. The standard coaxial

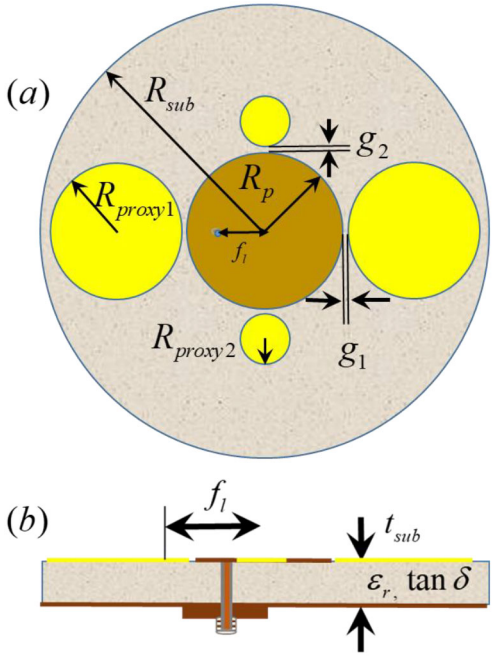

FIGURE 4. Proposed antenna model (a) top view and (b) bottom view.

TABLE 1. Optimized antenna design parameters (in millimeters).

R_{sub}	R_p	R_{proxy1}	R_{proxy2}	g_1	g_2	t_{sub}	f_l
76	23.25	22.90	10.19	0.98	0.15	1.57	7.41

SMA configuration is used to feed the antenna. The Antennas are designed and fabricated on Roger 5880 substrate with dielectric permittivity (ε_r) of 2.2 and loss tangent (tanδ) of 0.0009. The final antenna dimensions are tabulated in Table 1.

A detailed systematic design procedure, parametric sensitivity analysis, and comparison of measured and simulated results (viz. reflection coefficient and radiation pattern) of a unit antenna element are presented elsewhere in [39]. In this work, a 3×3 practical MIMO antenna configuration is investigated to enhance the channel capacity for HD video transmission. To position the antenna in MIMO configuration, the mutual coupling (isolation) between the antenna elements must be examined. The isolation between adjacent elements is measured under the following two configurations (co- and cross-polarization). The measured isolation results are shown in Figs. 5 and 6, respectively.

In the first configuration, where both antennas operate in the same polarization, the minimum distance for maintaining isolation $>$ 20 dB is found approximately 10 mm, as shown in Fig. 5. However, when the antennas operate in cross polarization, the minimum distance for maintaining isolation $>$ 30 dB in both bands is approximately 10 mm, as shown in Fig. 6. In the three-antenna MIMO configuration, the antennas are placed to maintain this minimum separation. In the proposed MIMO configuration shown in Fig. 7, the antenna elements are placed on the vertices of an

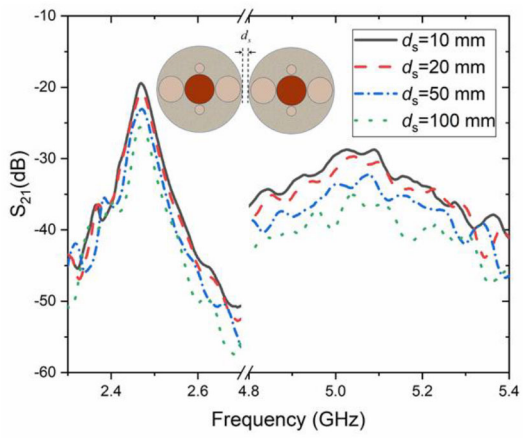

FIGURE 5. Isolation between antennas at different separation distances d_S (co-polarization).

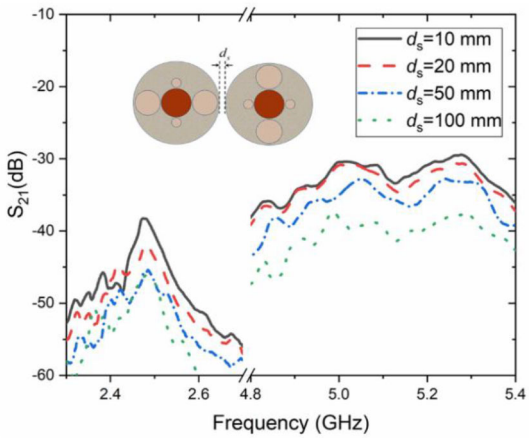

FIGURE 6. Isolation between antennas at different separation distances d_S (cross-polarization).

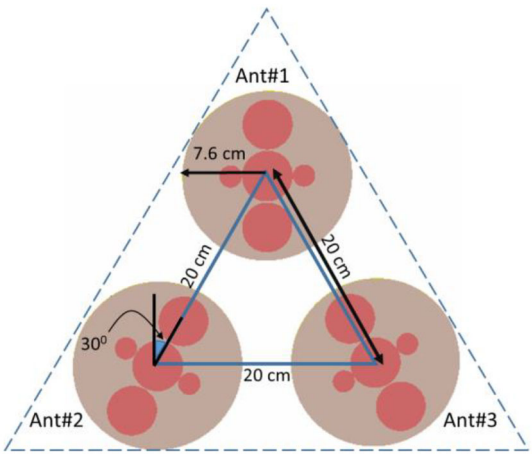

FIGURE 7. MIMO antenna array configuration.

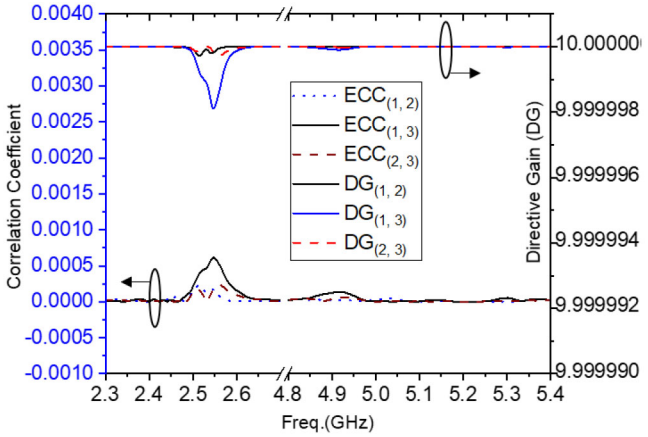

FIGURE 8. Correlation coefficients (ECC), directive gains (DG) for the proposed MIMO configuration.

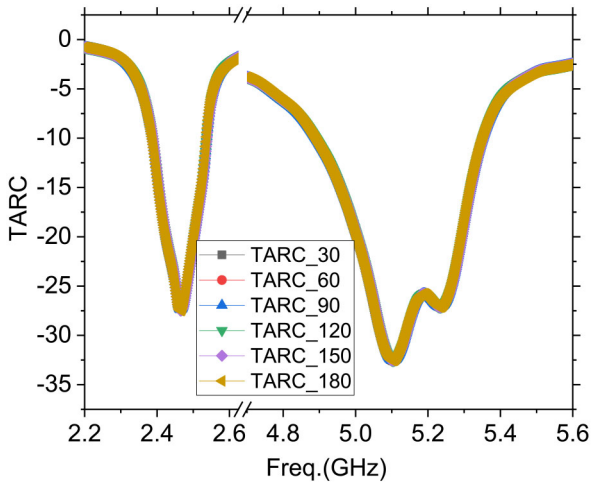

FIGURE 9. Total active reflection coefficient (TARC).

equilateral triangle of side 20 cm and an edge-to-edge separation of 48 mm. To achieve low correlation in the radiated fields, two antennas (i.e., Ant#2 and Ant#3) are rotated by 30 degrees in the clockwise and counter-clockwise direction, respectively, with respect to Ant#1.

Key MIMO parameters for the proposed configuration are estimated with the measured scattering parameters. Envelop Correlation Coefficient (ECC), Directive Gain (DG), and Total Active Reflection Coefficient (TARC) are calculated with the procedure given in [40] and plotted for both the frequency bands in Fig. 8 and Fig. 9. From Fig. 8, ECC is found to be below 0.0005, which is legitimately good isolation. As the correlation coefficient is well below 0.0005, the DG values are consistently around 10. The total active reflection coefficient (TARC) response for different phases shown in Fig. 9 indicates a decent MIMO configuration as it covers almost the similar −10dB bandwidths as of individual antenna without any significant deviation.

III. MEASUREMENTS AND FIELD EXPERIMENTS

A. LABORATORY VTS TESTING

To demonstrate real-time video transmission, the proposed VTS incorporates the 3-thin, semiflexible antennas as well as an HD camera, an SBC (Gateworks GW5530), and a

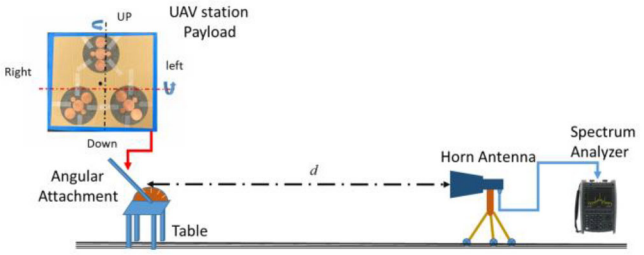

FIGURE 10. Setup for measuring the radiated power patterns of the MIMO antenna configuration.

Wi-Fi transceiver (doodle NM-DB-3) were assembled in the payload form shown in Figs. 2(c), (d). The platform was made of cardboard, and each component was attached using adhesive tape. The front view (Fig. 2(c)) shows the antennas placed in a triangular pattern forming an array and a camera in the center. The back view (Fig. 2(d)) shows the UAV electronics and battery. The testing of the VTS in real time was initially performed in a laboratory environment. The payload is shown in Fig. 2(b) was used as a UAV station. The three UWB-printed monopole antennas (instead of horn antennas) were attached to the ground station (based on the configuration shown in Fig. 3 for each channel of the RF transceiver). The MCS number was set to 3, which corresponds to a 16-quadrature amplitude modulation (16-QAM) scheme with a 1/2 coding ratio, and the RF transceiver was set for the maximum power output. A spectrum analyzer was used to measure the power transmitted by each RF channel of the transceiver. The maximum power transmitted from the RF transceiver that is being fed to the UAV antennas was approximately 18 dBm (i.e., $Ch_1 = 18.16$ dBm, $Ch_2 = 17.99$ dBm, and $Ch_3 = 18.4$ dBm) in the 2.4 GHz band. In the 5.2 GHz band, the measured maximum RF power from the transceiver was relatively lower at approximately 10 dBm ($Ch_1 = 10.04$ dBm, $Ch_2 = 9.92$ dBm, and $Ch_3 = 10.12$ dBm). To measure the maximum power transmitted from each individual channel, the spectrum analyzer was configured for a max-hold function. An average of 10 sample values was considered to estimate the RF power output.

B. RADIATED POWER PATTERN MEASUREMENT

The radiated power patterns were measured for the MIMO antenna configuration in an open field, where a table with a movable radial arm was used, as shown in Fig. 10. The UAV station was configured for the maximum power and was placed at a distance d (100 m in the 2.4-GHz band and 15 m in the 5.2-GHz band) from the ground station. The ground station comprised a horn antenna connected to a spectrum analyzer. The UAV payload was then rotated around the principal axes to cover the ±90° (up/down direction) elevation plane and ±90° (right/left direction) azimuth plane of the radiation hemisphere. The measured power levels for both frequency bands were plotted against the angle, as shown in Figs. 11 and 12. The active power pattern of the

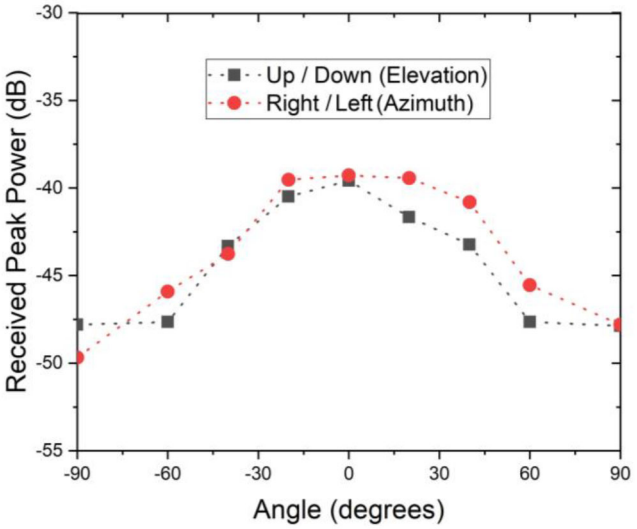

FIGURE 11. Power pattern of the MIMO antenna array measured for the configuration shown in Fig. 7 for operation in the 2.4-GHz band.

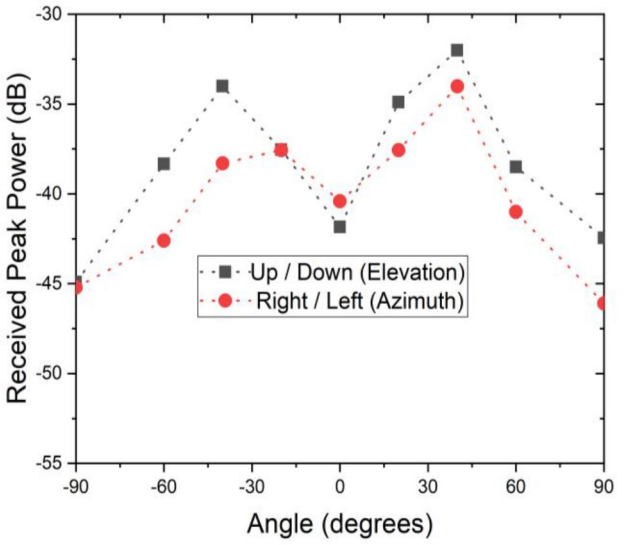

FIGURE 12. Power pattern of the MIMO antenna array measured for the configuration shown in Fig. 7 for operation in the 5.2-GHz band.

MIMO antenna array exhibited broadside radiation coverage on both the principal axes in the 2.4-GHz band; however, in the 5.2-GHz band, it showed a null in the broadside direction suggesting a quasi-isotropic behavior.

C. FIELD EXPERIMENT: GROUND-TO-GROUND TRANSMISSION

The communication range of the proposed system was tested for a ground-to-ground transmission scenario. The ground station, which comprised 3-high-gain horn antennas (Fig. 3(b)) and the payload (Figs. 2 (c) and (d)), was carried by a team member along the terrain shown in Fig. 13. In the ground-to-ground transmission tests, the channel throughput was measured for different distances (300, 500, 700, and 900 m) for operation in both frequency bands. The achieved

FIGURE 13. Map view of the terrain considered for field experiments.

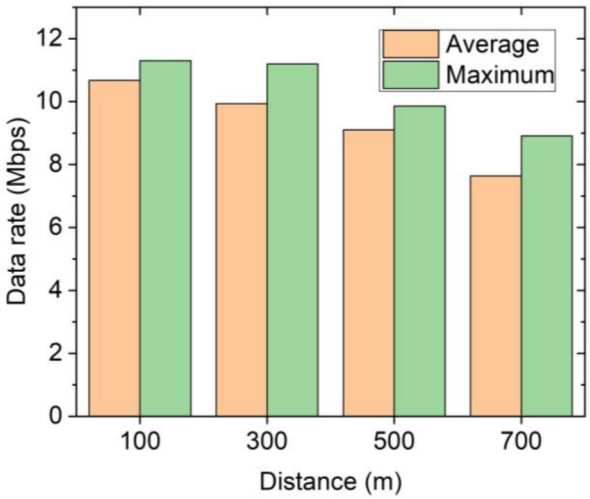

FIGURE 14. Measured data rate of the MIMO antenna array of the configuration shown in Fig. 10 operating in the 2.4-GHz band.

data rates of the proposed MIMO configuration are presented in Figs. 14 and 15. The real-time HD video was successfully received up to 2.70-km and 840-m distances for operation in the 2.4- and 5.2-GHz bands, respectively. The received signal strength measured at the ground station for a stable HD video stream received from the camera installed in the payload was approximately −72 dBm for operation in both frequency bands.

D. FIELD EXPERIMENT: AIR-TO-GROUND TRANSMISSION

The communication range of the proposed system was also tested for an air-to-ground transmission scenario. The payload platform was placed on the drone based on the configurations shown in Fig. 16 to assess the system performance under different mounting conditions. Using this setup, a ground station employing three high-gain directive horn antennas was established at the point shown in Fig. 13. The HD video stream was successfully received at approximately 3.56 km from the ground station at a very low altitude of ≥50 m for operation in the 2.4-GHz band. The

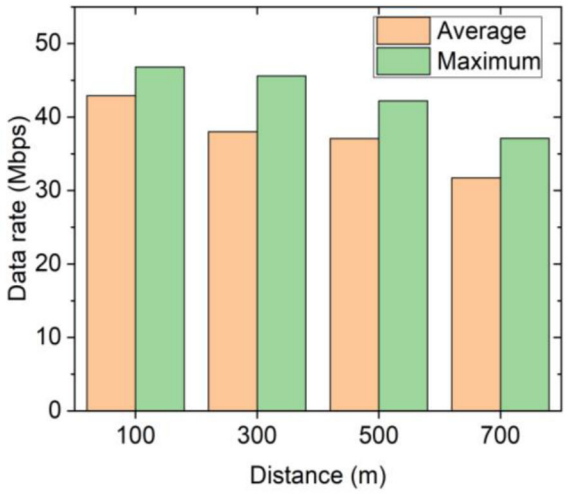

FIGURE 15. Measured data rate of the MIMO antenna array of the configuration shown in Fig. 10 operating in the 5.2-GHz band.

measured signal strength for each channel at the ground station was approximately −72 dBm. However, in the 5.2-GHz band, the HD video stream was successfully received at ∼1 km at a very low altitude of ≥50 m with the measured signal strength of approximately −70 dBm for each channel. The reason for the shorter communication range in the 5.2-GHz band than in the 2.4-GHz band is due to the low output power from the RF transceiver in the 5.2-GHz band (i.e., 8 dB below the 2.4-GHz output power) and the large free space path loss, which is expected owing to the high operating frequency.

The performance of the proposed HD video transmission system is compared with a few commercial solutions available in the market as shown in Table 2. After careful comparison with the specs available from various manufacturers, it is found that the proposed VTS is providing a decent data rate, which indicates high-quality video transmission. In addition, our system is utilizing the semi-flexible dual mode high gain MIMO antenna systems that can provide seamless integration with the UAV body while all the commercial solutions are employing the vertically mounted monopole antennas of low gains. In conclusion, our solution shows performance in a real scenario (not ideal like some commercial companies show), we are the only solution with dual switchable bands operation, and we are showing the highest data rate and comparable range with the lowest transmitted power.

IV. CONCLUSION

An indigenously developed HD VTS was tested in open field conditions. The proposed system uses a three-element triangular array of thin, semi-flexible antennas, particularly designed for wide bandwidth and coverage. The active power pattern of the proposed array was obtained in the radiation hemisphere to determine the coverage. A full system characterization was initially performed in a laboratory environment, and the power levels were measured for each

TABLE 2. Comparison of proposed VTS specs with commercial solutions.

#	Particular	Frequency (GHz)	Power Transmitted (dBm)	Range (Km)	Date rate (Max)	Video resolution	Seamless Antenna	Dual-band Switchable	MIMO
[41]	DJI FPV	5.725-5.850	30/19/14	4/2.5/0.7	-	720p	NO	NO	NA*
[42]	Caddx Vista Digital	5.725-5.850	30/14	4/0.7	-	720p	NO	NO	NA*
[43]	VDC-7 Long Range Video Transmission System	2.4	25	7	~ 5Mbps	1080p	NO	NO	NA*
[44]	Herelink 2.4 GHz Long Range HD Video Transmission System	2.4	-	20*	-	1080p	NO	NO	NA*
[45]	DVL-C Long Range HD Video Transmission System	5	20/29	0.8/3	-	1080p	NO	NO	NA*
This work	Proposed Video Transmission System	2.4, 5170–5330	18 @2.4GHz 10@5.2 GHz	3.57/0.970⁺	~8 Mbps ~30 Mbps	720p	Yes	Yes 2.4/5.2 GHz	3

NA*: Information is not available

FIGURE 16. Payload attachment on the UAV (a) vertical and (b) horizontal orientation.

channel for operation in two frequency bands. Next, the UAV module was placed on a commercial drone, and an HD video stream was received at a remote ground station for operation in both frequency bands. It was found that the proposed VTS could establish an HD video link between a UAV and ground station at distances of 3.56 km and ∼1.0 km for operation in the 2.4- and 5.2-GHz bands, respectively.

ACKNOWLEDGMENT

This work was supported by Lockheed Martin Corporation at the Integrated Microwave Packaging Antenna and Circuits Lab, King Abdullah University of Science and Technology, Kingdom of Saudi Arabia.

REFERENCES

[1] E. Cheng, *Aerial Photography and Videography Using Drones*. San Francisco, CA, USA: Peachpit Press, 2015.

[2] D. Câmara, "Cavalry to the rescue: Drones fleet to help rescuers operations over disasters scenarios," in *Proc. IEEE Conf. Antenna Meas. Appl. (CAMA)*, 2014, pp. 1–4.

[3] Y. Karaca *et al.* "The potential use of unmanned aircraft systems (drones) in mountain search and rescue operations," *Amer. J. Emerg. Med.*, vol. 36, no. 4, pp. 583–588, 2018.

[4] P. Molina *et al.* "Drones to the rescue!" Inside GNSS. Jul./Aug. 2012. [Online]. Available: https://infoscience.epfl.ch/record/180464

[5] U. R. Mogili and B. B. V. L. Deepak, "Review on application of drone systems in precision agriculture," *Procedia Comput. Sci.*, vol. 133, pp. 502–509, Jan. 2018.

[6] P. Tokekar, J. V. Hook, D. Mulla, and V. Isler, "Sensor planning for a symbiotic UAV and UGV system for precision agriculture," *IEEE Trans. Robot.*, vol. 32, no. 6, pp. 1498–1511, Dec. 2016.

[7] S. Marathe, "Leveraging drone based imaging technology for pipeline and RoU monitoring survey," in *Proc. SPE Symp. Asia Pacific Health, Safety, Security, Environ. Social Responsibility*, 2019, Art. no. SPE-195427-MS.

[8] O. Menéndez, M. Pérez, and F. A. Cheein, "Visual-based positioning of aerial maintenance platforms on overhead transmission lines," *Appl. Sci.*,vol. 9, no. 1, p. 165, 2019.

[9] J. C. Hodgson *et al.*, "Drones count wildlife more accurately and precisely than humans," *Methods Ecol. Evol.*, vol. 9, no. 5, pp. 1160–1167, 2018.

[10] J. Linchant, J. Lisein, J. Semeki, P. Lejeune, and C. Vermeulen, "Are unmanned aircraft systems (UASs) the future of wildlife monitoring? A review of accomplishments and challenges," *Mammal Rev.*, vol. 45, no. 4, pp. 239–252, 2015.

[11] Q. Wang, J. Gu, H. Huang, and Y. Zhao, "Online drone-based moving target detection system in dense-obstructer environment," in *Proc. IEEE 24th Int. Conf. Parallel Distrib. Syst. (ICPADS)*, 2018, pp. 860–867.

[12] K. M. Hasan, S. H. S. Newaz, and M. S. Ahsan, "Design and development of an aircraft type portable drone for surveillance and disaster management," *Int. J. Intell. Unmanned Syst.*, vol. 6, pp. 1–15, May 2018.

[13] T. Wall and T. Monahan, "Surveillance and violence from afar: The politics of drones and liminal security-scapes," *Theor. Criminol.*, vol. 15, no. 3, pp. 239–254, 2011.

[14] G. S. McNeal, "Drones and the future of aerial surveillance," *George Washington Law Rev.*, vol. 84, p. 354, Mar. 2016.

[15] P. Pathak, M. Damle, P. R. Pal, and V. Yadav, "Humanitarian impact of drones in healthcare and disaster management," *Int. J. Recent Technol. Eng.*, vol. 7, no. 5, pp. 201–205, 2019.

[16] M. Erdelj, E. Natalizio, K. R. Chowdhury, and I. F. Akyildiz, "Help from the sky: Leveraging UAVs for disaster management," *IEEE Pervasive Comput.*, vol. 16, no. 1, pp. 24–32, Jan.–Mar. 2017.

[17] G. Ling and N. Draghic, "Aerial drones for blood delivery," *Transfusion*, vol. 59, no. S2, pp. 1608–1611, 2019.

[18] E. Ackerman and E. Strickland, "Medical delivery drones take flight in east africa," *IEEE Spectrum*, vol. 55, no. 1, pp. 34–35, Jan. 2018.

[19] R. Deng, J. He, M. Chen, Y. Wei, J. Shi, and L. Chen, "Real-time VLLC-OFDM HD-SDI video transmission system with TS-based SFO estimation," in *Proc. Opt. Fiber Commun. Conf. Exhibition (OFC)*, 2017, pp. 1–3.

[20] J. Guo, X. Li, Z. Lv, Y. Yang, and L. Li, "Design of real-time video transmission system for drone reliability," in *Proc. IOP Conf. Series Mater. Sci. Eng.*, vol. 790, 2020, Art. no. 12004.

[21] W. Kim, "Design of hybrid communication structure for video transmission in drone systems," *J. Korea Converg. Soc.*, vol. 10, no. 11, pp. 9–14, 2019.

[22] Q. Yang and J. H. Yang, "HD video transmission of multi-rotor unmanned aerial vehicle based on 5G cellular communication network," *Comput. Commun.*, vol. 160, pp. 688–696, Jul. 2020.

[23] W. Zhou. "High definition, low delay, SDR-based video transmission in UAV applications." Analogdialogue. Jan. 2017. [Online]. Available: https://www.analog.com/en/analog-dialogue/articles/high-definition-low-delay-sdr-based-video-transmission-in-uav-applications.html
[24] A. M. Hayajneh, S. A. R. Zaidi, D. C. McLernon, and M. Ghogho, "Optimal dimensioning and performance analysis of drone-based wireless communications," in *Proc. IEEE Globecom Workshops (GC Wkshps)*, 2016. pp. 1–6.
[25] J. Supramongkonset, S. Duangsuwan, and S. Promwong, "A WiFi link budget analysis of drone-based communication and IoT ground sensors," in *Proc. 7th Int. Conf. Eng. Appl. Sci. Technol. (ICEAST)*, 2021, pp. 234–237.
[26] E. Yanmaz, R. Kuschnig, and C. Bettstetter, "Channel measurements over 802.11 a-based UAV-to-ground links," in *Proc. IEEE GLOBECOM Workshops (GC Wkshps)*, 2011, pp. 1280–1284.
[27] M. Nosrati, A. Jafargholi, R. Pazoki, and N. Tavassolian, "Broadband slotted blade dipole antenna for airborne UAV applications," *IEEE Trans. Antennas Propag.*, vol. 66, no. 8, pp. 3857–3864, Aug. 2018.
[28] J. Tak and J. Choi, "A flush-mounted monopolar patch antenna for UAV applications," *Microw. Opt. Technol. Lett.*, vol. 59, no. 5, pp. 1202–1207, 2017.
[29] L. Sun, B.-H. Sun, Q. Sun, and W. Huang, "Miniaturized annular ring slot antenna for small/mini UAV applications," *Progr. Electromagn. Res.*, vol. 54, pp. 1–7, Oct. 2014.
[30] S. Yoon, J. Tak, J. Choi, and Y. Park, "Conformal monopolar antenna for UAV applications," in *Proc. IEEE Int. Symp. Antennas Propag. USNC/URSI Nat. Radio Sci. Meeting*, 2017, pp. 517–518.
[31] L. I. Balderas, A. Reyna, M. A. Panduro, C. Del Rio, and A. R. Gutiérrez, "Low-profile conformal UWB antenna for UAV applications," *IEEE Access*, vol. 7, pp. 127486–127494, 2019.
[32] Z.-Q. Liu, Y.-S. Zhang, Z. Qian, Z. P. Han, and W. Ni, "A novel broad beamwidth conformal antenna on unmanned aerial vehicle," *IEEE Antennas Wireless Propag. Lett.*, vol. 11, pp. 196–199, 2012.
[33] D. Ammous, F. Kammoun, and N. Masmoudi, "Analysis of coding and transfer of arien video sequences from H.264 standard," in *Proc. 5th Int. Conf. Adv. Technol. Signal Image Process. (ATSIP)*, 2020, pp. 1–5.
[34] T. Brown, B. Argrow, C. Dixon, S. Doshi, R.-G. Thekkekunnel, and D. Henkel, "Ad hoc UAV ground network (AUGNet)," in *Proc. AIAA 3rd Unmanned Unlimited Tech. Conf. Workshop Exhibit*, 2004, pp. 1–11.
[35] R. Muzaffar, E. Yanmaz, C. Raffelsberger, C. Bettstetter, and A. Cavallaro, "Live multicast video streaming from drones: An experimental study," *Auton. Robots*, vol. 44, no. 1, pp. 75–91, 2020.
[36] B. J. O. De Souza and M. Endler, "Coordinating movement within swarms of UAVs through mobile networks," in *Proc. IEEE Int. Conf. Pervasive Comput. Commun. Workshops (PerCom Workshops)*, 2015, pp. 154–159.
[37] G. N. Solidakis *et al.*, "An arduino-based subsystem for controlling UAVs through GSM," in *Proc. 6th Int. Conf. Modern Circuits Syst. Technol. (MOCAST)*, 2017, pp. 1–4.
[38] S. Qazi, A. S. Siddiqui, and A. I. Wagan, "UAV based real time video surveillance over 4G LTE," in *Proc. Int. Conf. Open Source Syst. Technol. (ICOSST)*, 2015, pp. 141–145.
[39] Z. Akhter, R. M. Bilal, and A. Shamim, "A dual mode, thin and wideband MIMO antenna system for seamless integration on UAV," *IEEE Open J. Antennas Propag.*, vol. 2, pp. 991–1000, 2021.
[40] M. S. Sharawi, *Printed MIMO Antenna Engineering*. Boston, MA, USA: Artech House, 2014.
[41] "DJI Digital FPV System." Jun. 24, 2022. [Online]. Available: https://www.dji.com/fpv/info#specs
[42] "Caddx Vista Digital HD System for DJI." Jun. 24, 2022. [Online]. Available: https://www.getfpv.com/caddx-vista-digital-hd-system-for-dji-hd-fpv.html
[43] "VDC-7/VDC-15 Long Range Video/Data/RC Transmission System." Jun. 24, 2022. [Online]. Available: https://www.foxtechfpv.com/vdc-long-range-video-data-radio-transmission-system.html
[44] "Herelink 2.4GHz Long Range HD Video Transmission System." Jun. 24, 2022. [Online]. Available: https://www.foxtechfpv.com/herelink-2-4ghz-long-range-hd-video-transmission-system.html
[45] "DVL-C Long Range HD Video Transmission System with Camera." Jun. 25, 2022. [Online]. Available: https://www.foxtechfpv.com/dvl-c-long-range-hd-video-transmission-system.html